Study of Correlation Effects in the High Formal Oxidation State Compound Sr_2CoO_4

K.-W. Lee and W. E. Pickett
Department of Physics, University of California, Davis, California 95616, USA
(Dated: February 23, 2006)

Two recent reports confirm that the newly synthesized Sr_2CoO_4 (formal oxidation state Co^{4+}) shows a high Curie temperature ($\sim$ 250 K), but they report different moments of 1.8 μ_B and 1 μ_B per Co. Using both commonly used functionals in the correlated band approach (LDA+U) as well as the local density approximation (LDA), the combined effects of correlation and hybridization with O $2p$ states are calculated and analyzed. Sr_2CoO_2 is already ferromagnetic within LDA (M=1.95 μ_B). Increasing U from zero, the two LDA+U schemes affect the moment oppositely out to a critical value U_c=2.5 eV, at which point they transform discontinuously from different states to the *same* large U state. Fixing U at U_c, fixed spin moment calculations show similar behavior out to a minimum at $1\mu_B$ (a half metallic state), beyond which the fully-localized-limit scheme jumps to a state with energy minimum very near $2\mu_B$ (very close to the LDA moment). Although the energy minima occur very near integer values of the moment/Co ($1\mu_B, 2\mu_B$), the strong $3d-2p$ mixing and resulting $3d$ orbital occupations seem to preclude any meaningful $S=\frac{1}{2}$ or $S=1$ assignment to the Co ion.

PACS numbers: 71.20.Be, 71.27.+a, 71.30.+h, 75.30.Gw

I. INTRODUCTION

First row ($3d$) transition metal ions in high oxidation states have been of interest for some time, due to their competing and delicate spin states. There are still several cases where behavior is not understood, indeed sometimes (due to sample questions arising from difficulty in synthesis) the data is not unambiguous. The best known, and most thoroughly studied, example is that of the quasi-two-dimensional (2D) cuprates, which when hole-doped become high temperature superconductors. In their undoped state they are Cu^{2+}-based antiferromagnetic insulators. Hole doping drives the Cu oxidation state toward the unstable (practically non-existent) Cu^{3+} state. At a doping level of 0.15-0.20 holes/Cu optimal superconductivity is reached. They can be doped beyond that level, when they become conventional metallic Fermi liquids. Upon hole doping the 'oxidation state' designation must be interpreted with care, since it is clear that the holes go onto the oxygen ions to a large degree.

Another high-oxidation-state ion is Co^{4+}. This ion has recently gained wide exposure due to the unusual properties of Na_xCoO_2, including the discovery[1] that this system becomes superconducting (4.5 K) around x=0.3 when it is hydrated. This value of x suggests that the Co ion is 70% of the way to being Co^{4+}, or alternatively, 70% of the ions are Co^{4+} while 30% are Co^{3+}. This system is however metallic for all x except for Na ion/orbital/spin/charge ordering[2] precisely at x=0.5 (precisely what is responsible is not yet clear). There is magnetism and correlated electron behavior for $x > 0.5$ (the Co^{3+} end) while for $x < 0.5$ the materials appear to be weakly correlated nonmagnetic metals. While there has been much expectation that the (metastable) endpoint member CoO_2 (nominally Co^{4+}, d^5) is a Mott insulator, the evidence is that it remains a nonmagnetic metal.[3] Calculations indicate[4] that, as in the cuprates, upon hole doping from the Co^{3+} end, much of the charge difference occurs on the O ion.

The $La_{2-x}Sr_xCoO_4$ system (LSCoO) with two-dimensional layered K_2NiF_4 structure has become interesting because of its magnetic and electrical properties. In this system the formal oxidation state $Co^{(2+x)+}$ near the La end is not unusually high, so its behavior might be expected to be readily understandable. With increasing Sr concentration x, LSCoO shows a structural transition from orthorhombic to tetragonal (i.e., a lattice constant $b \rightarrow a$) around x=0.5, with enhanced two-dimensional electronic properties.[5] The structural transition may be connected to an antiferromagnetic-ferromagnetic transition (the maximum Curie temperature T_C=220 K at x=0.9),[6] accompanying a magnetic change that has been interpreted in terms of a Co^{3+} spin-state transition from high spin to intermediate spin configurations around x=0.7.[7] There is another suggestion that at x=1 the system is a high-spin, low-spin charge-ordered state.[8] However, there is no agreement amongst the measurements on the magnetic behavior [6, 9–11] nor metallic behavior[6, 12]. The end member x=0 is an antiferromagnetic (AFM) insulator with Neel temperature T_N=275 K.[13]

Although earlier studies were confined to the

range below x=1.4, recently the end member Sr_2CoO_4, formally Co^{4+}, was synthesized by Matsuno *et al.*[14, 15] and by Wang *et al.*[16, 17], and characterized as FM with high Curie temperature $T_C \approx 250$ K. However, their differing synthetic methods have led to different properties. Matsuno *et al.* synthesized a single-crystalline thin film using pulsed-laser deposition, while Wang *et al.* produced polycrystalline samples under high pressure, high temperature conditions. The former shows metallic T-dependent resistivity below T_C, although it has definitely higher resistivity of order of $10^{-4} - 10^{-3}$ Ω cm at low T than in a typical metal. The pressure-synthesized samples show nearly temperature independent resistivity (perhaps due to polycrystallinity), but with similar magnitude. The more confusing difference is in the observed saturation magnetic moment, 1.8 μ_B and 1 μ_B/Co respectively. Nevertheless, the sample with the smaller ordered moment has been observed[16] effective (Curie-Weiss) moment p_{eff}= 3.72 μ_B, characteristic of a much higher $S = 3/2$ spin configuration. Such a moment would suggest a much higher ordered moment, $< S_x > \sim 3\mu_B$.

The related perovskite system $La_{1-x}Sr_xCoO_3$ (formally $Co^{(3+x)+}$) has been studied for some time.[18–24] Its magnetic properties are also altered by Sr concentration x: nonmagnetic for $x < 0.05$, spin glass for $0.05 \leq x < 0.2$, and ferromagnetic above x=0.2. For the end member, $SrCoO_3$ ("Co^{4+}") shows metallic conductivity and has magnetic moments 1.25 and 0.1 μ_B for Co and O respectively,[18] whereas the ground state of $LaCoO_3$ is a nonmagnetic band insulator. Its excitations have been interpreted in terms of a locally orbitally-ordered excited state.[24, 25]

In this paper, we look in some detail at the electronic and magnetic structure of Sr_2CoO_4 both as uncorrelated, using the local density approximation (LDA), and viewing effects of correlation as described by the LDA+Hubbard U (LDA+U) method. Both commonly used LDA+U functionals are employed, and their results are compared and contrasted. A number of unusually rich magnetic phenomena arise (including a half metallic phase), reflecting the strong hybridization with O $2p$ states that complicates the accommodation of correlation effects on the Co ion.

II. STRUCTURE AND CALCULATION

Sr_2CoO_4 has the bct K_2NiF_4-type structure, space group $I4/mmm$ (No. 139), pictured in Fig. 1. The Co - planar O (PO) bond length (1.878 Å) is shorter by about 6% than that of Co - apical O (AO) (1.988 Å). The distorted CoO_6 octahedron, elongated along c-axis, leads to crystal field splitting of $t_{2g} \rightarrow E_g(d_{xz}, d_{yz}) + B_{2g}(d_{xy})$ and $e_g \rightarrow A_g(d_{3z^2-r^2}) + B_{1g}(d_{x^2-y^2})$ states. We have used the lattice constants a=3.755 Å, c=12.6 Å, and apical O (0.1578) and Sr (0.3544) internal parameters optimized by Matsuno *et al.*,[14] which are consistent with the experimentally measured values by Wang *et al.*[16]

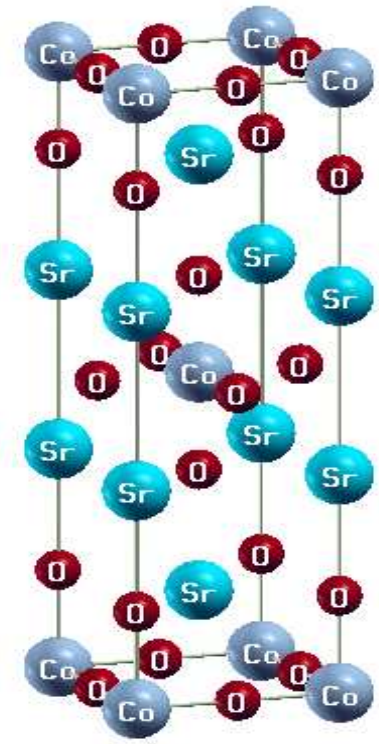

FIG. 1: (Color online) Crystal structure of Sr_2CoO_4, a body-centered-tetragonal type. The planar O-Co bond length is 1.878 Å, about 6% shorter than the apical O-Co bond length. Lattice constants used here are a=3.755 Å and c=12.6 Å.

Our calculations were carried out within the local density approximation (LDA) and LDA+U approaches with the full-potential nonorthogonal local-orbital (FPLO) method.[27] Both commonly used schemes of the LDA+U method were employed so comparisons of the predictions could be made. Both forms have the same Hubbard-like density-density interaction

$$E_U = \frac{1}{2} \sum_{m\sigma \neq m'\sigma'} [U_{mm'} - \delta_{\sigma,\sigma'} J_{mm'}] n_{m\sigma} n_{m'\sigma'} \quad (1)$$

where $\{n_{m\sigma}\}$ is a site occupation set and J is intra exchange integral. The form displayed here is schematic in the sense that it does not display all of the indices involved in the full coordinate-

system-independent form that is implemented in the code. The two LDA+U approaches differ only in the method of treatment of the "double counting" term, intended to subtract out the shell-averaged interaction that has already been included in LDA. One choice is the so-called "around mean field" (AMF) scheme, which is expected to be more suitable when the on-site Coulomb repulsion U is not so strong.[28] The other choice, called the "fully localized limit" (FLL) (also called "atomic limit"), is more appropriate for large U systems.[29] The methods to treat the double counting problem in the both schemes are given by

$$E^{dc}_{AMF} = \frac{1}{2} \sum_{m\sigma \neq m'\sigma'} [U_{mm'} - \delta_{\sigma,\sigma'} J_{mm'}] \; \bar{n} \; \bar{n}, \quad (2)$$

$$E^{dc}_{FLL} = \frac{1}{2} \sum_{m\sigma \neq m'\sigma'} [U_{mm'} - \delta_{\sigma,\sigma'} J_{mm'}] \bar{n}_\sigma \bar{n}_{\sigma'},$$

where $\bar{n}$ is the shell-averaged occupation, while $\bar{n}_\sigma$ is its spin-decomposed analog. These double-counting terms can be written in other forms that emphasize other aspects of the interaction.[30] However, this form is illustrative because it emphasizes that the difference lies in the magnitude of the (self-consistent) atomic moment. Clearly it is only the spherically averaged values of U and J that enter the double-counting terms. The difference between the two forms is that the double-counting term, and the resulting potential, includes a spin dependence in the FLL form.

The fully relativistic scheme of FPLO[31] was used when spin-orbit coupling (SOC) in LDA was necessary. The choice of basis orbitals were Sr $(4s4p)5s5p4d$, Co $(3s3p)4s4p3d$, and O $2s2p(3s3p3d)$. (The orbitals in parentheses indicate semi-core or polarization orbitals.) The Brillouin zone was sampled by a regular mesh containing up to 641 irreducible **k** points for LDA and LDA+U, and 1639 irreducible **k** points for SOC and fixed spin moment (FSM)[32] calculations that require more carefully treatment near the Fermi level (E_F).

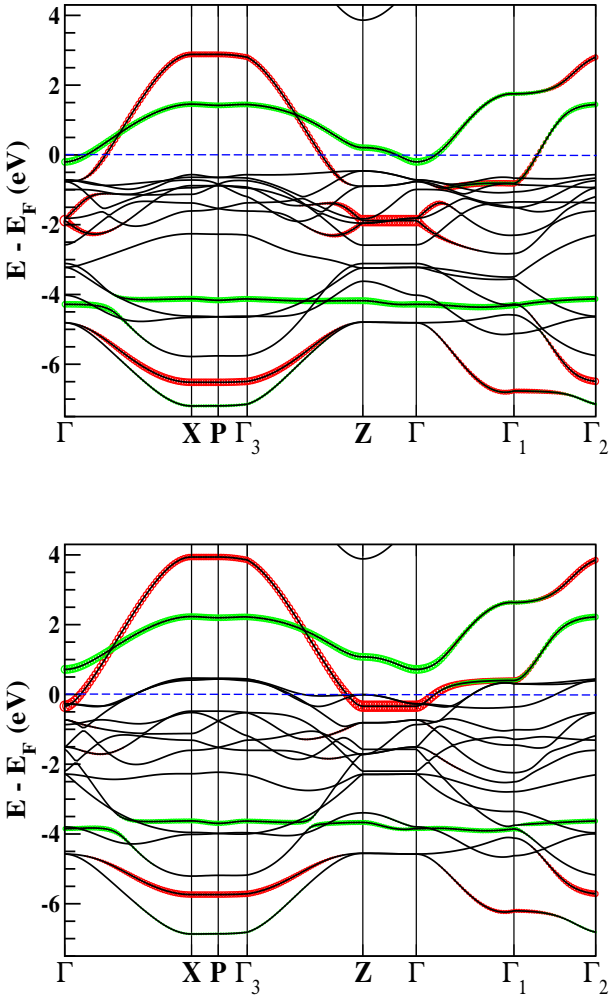

FIG. 2: (Color online) FM LDA majority (upper) and minority (lower) band structures along symmetry directions. The thickened (and colored) lines emphasize Co $d_{3z^2-r^2}$ (green or light) and $d_{x^2-y^2}$ (red or black) characters, which form bonding and antibonding bands with apical and in-plane O p_σ states respectively. The symmetry points for the body-centered-tetragonal structure follow the Bradley and Cracknell notation as given in Fig. 6. The dashed horizontal line denotes the Fermi energy.

III. UNCORRELATED TREATMENT

A. Electronic structure

The FM LDA band structures, exhibiting total magnetic moment M=1.95 μ_B that is only accidentally near an integer value, are shown in Fig. 2. The five Co $3d$ bands and three $2p$ bands of each O constitute an entanglement of 17 hybridized bands for each spin, with total $p-d$ bandwidths of 10 eV and 11 eV for the majority and minority bands respectively. The strong hybridization throughout the bands is evident in the corresponding total DOS and accompanying atom-projected DOS, shown in Fig. 3. The crystal field splitting of 2 eV, identified from the density of states, between t_{2g} and e_g manifolds is only a little higher than the exchange splitting 1.3 eV. As noted earlier, these t_{2g} and e_g designations are broken down by the $4/m$ symmetry of the Co site. The electronic structure shows clear quasi-two-dimensionality, consistent with resistivity measurement by Matsuno *et al.*

In Fig. 2, the $pd\sigma$ and $pd\sigma^*$ bands (for each of $d_{x^2-y^2}$ and $d_{3z^2-r^2}$ orbitals) are highlighted. The

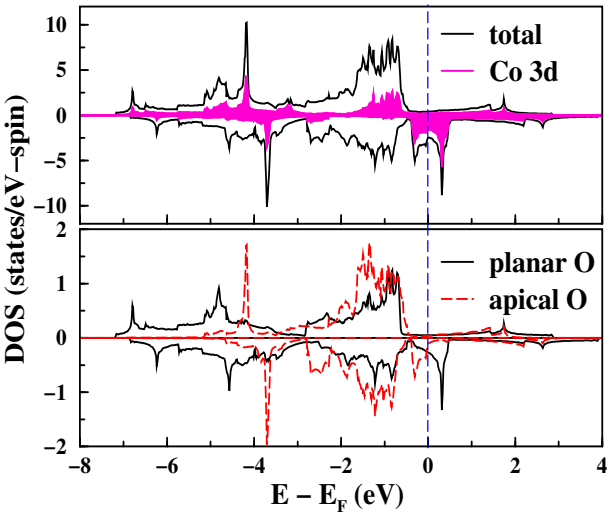

FIG. 3: (Color online) Total and atom-projected densities of states for LDA FM calculation. Near E_F, there is a van Hove singularity in the minority channel. While AO is almost fully occupied, the minority of PO is partially occupied, resulting in large magnetic moment for PO (for details, see text). Additionally, the band width of AO is by 40% less than that of PO. The DOS at E_F $N(0)$ is 2.90 states/eV per both spins.

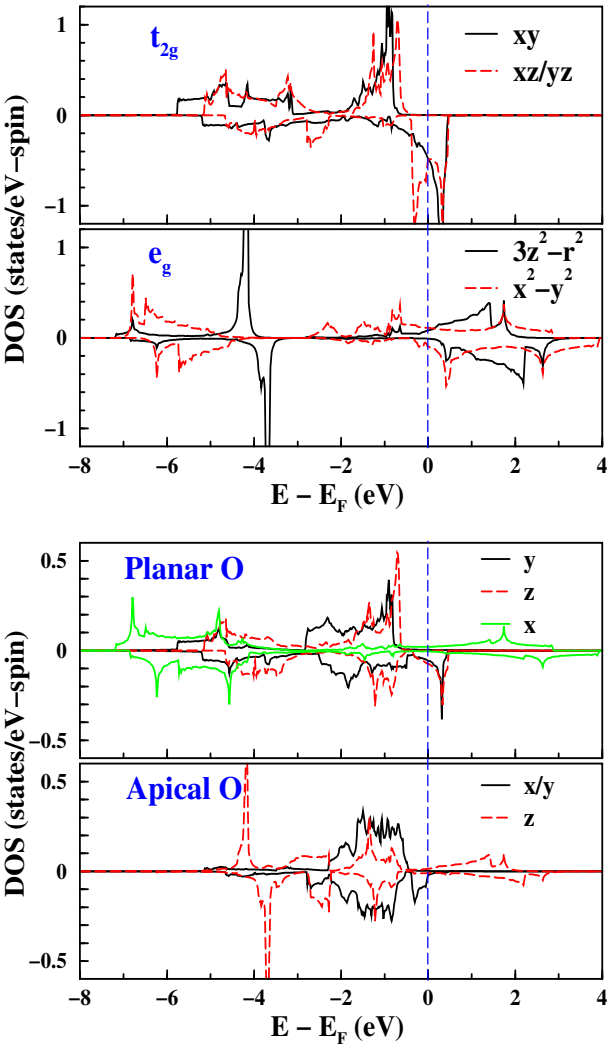

FIG. 4: (Color online) Orbital-projected densities of states for Co 3d (upper) and O p states (lower) in LDA FM calculation. The d_{xz} and d_{yz} states are degenerate. The crystal field splitting of 2 eV between t_{2g} and e_g manifolds is only a little higher than the exchange splitting 1.3 eV. The PO p_x and AO p_z are the σ-orbital.

more dispersive bands (darker, or red) arise from bonding and antibonding interactions between Co $d_{x^2-y^2}$ and PO p_σ states. The bonding and antibonding bands have a separation of 10 eV at the X point, this total width arising from a combination of the differences between the t_{2g} and $2p$ site energies, and the hybridization between them. The dispersion of the antibonding (upper) band can be described roughly by effective hopping amplitude $t = 0.40$ eV (majority) and $t = 0.53$ eV (minority). The behavior of the $d_{x^2-y^2}$ band is similar to that observed in the high T_c superconductor La_2CuO_4, in which this antibonding band plays a central role,[33, 34] but it is mostly unoccupied here. However, with the lower number of 3d electrons the cobaltate electronic structure is influenced more strongly by the t_{2g} manifold, which forms relatively flat bands, the top of which hovers around the Fermi energy. In the minority bands a van Hove singularity lies at E_F at the Z point, perhaps contributing to the positioning of the Fermi level and hence to the total moment.

The less dispersive highlighted bands (green, or lighter), lying in the 0 - 2 eV range, arise from the antibonding interaction of Co $d_{3z^2-r^2}$ and AO p_σ states. The bonding band of this pair consists of a remarkably flat band at -4 eV for each spin direction.

B. Magnetic Tendency

The FM state is favored energetically over the nonmagnetic state by 0.37 eV/Co, similar to the value given by Matsuno *et al.* The spin magnetic moments are 1.95 total, 1.52 from Co and 0.22 from each PO (in units of μ_B). The large magnetic moment for PO, due to strong hybridization with Co 3d bands, has been observed previously in Li_2CuO_2[36] and a few other cuprates. The Mullikan decomposition of O charges as well as the band filling of related bands indicates that AO is consistent with its formal designation O^{2-}, whereas PO contributes con-

TABLE I: Co $3d$ orbital (Mullikan) occupancy in LDA, where M=1.95 μ_B. The difference of occupancies between both spin channels is directly related with contribution of each orbital to spin magnetic moment, which can be seen to be spread over all five $3d$ orbitals.

	t_{2g}			e_g	
	E_g		B_{2g}	A_g	B_{1g}
	xz	yz	xy	$3z^2-r^2$	x^2-y^2
majority	1.00	1.00	1.00	0.56	0.67
minority	0.68	0.68	0.54	0.36	0.32
difference	0.32	0.32	0.46	0.20	0.35

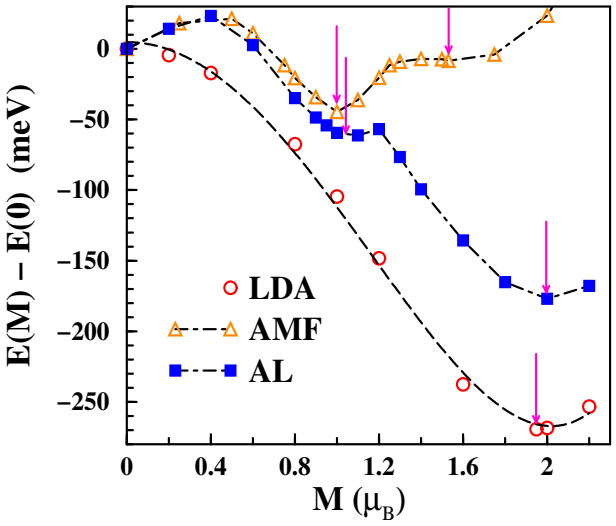

FIG. 5: (Color online) Fixed spin moment calculations in LDA and both LDA+U schemes at U_c=2.5 eV. The arrows pinpoint (meta)stable states. The dashed line for LDA FSM indicates fitting line with $E(M)-E(0) = \varepsilon_0 - \alpha M^2 + \beta M^4$, where ε_0=5 meV, α=133 meV/μ_B^2, and β=16 meV/μ_B^4.

siderably to the conduction bands and cannot be considered fully ionic. According to the Co $3d$ orbital occupancies given in Table I, however, every $3d$ orbital contributes to the magnetic moment due to itineracy. The variation from average contribution occurs in two states: d_{xy} has 40% larger, and $d_{3z^2-r^2}$ orbital 40% smaller, contributions than the average contribution to the moment. The strong itinerant character (all $3d$ orbitals are neither fully occupied nor fully unoccupied) explains why no Jahn-Teller distortion is observed in Sr_2CoO_4.

The fixed spin moment method[32] is applied in a following subsection to probe the magnetic behavior. In the LDA fixed spin moment calculations the low moment region is given by $E(M)-E(0) \approx -\alpha M^2+\beta M^4$ with constants α=133 meV/μ_B^2, β=16 meV/μ_B^4. The Stoner-enhanced susceptibility is given by

$$\chi = \chi_0/[1-N(0)I] \qquad (3)$$

where the bare susceptibility $\chi_0 = 2\mu_B^2 N(0)$ and $N(0)$ is the single-spin density of states at the Fermi level. Also in the low-M limit one obtains formally $\alpha = (1/2)\chi^{-1}$, giving the Stoner interaction I = 1.17($\pm$0.05) eV. With this value $IN(0)\approx$ 1.7, giving a very strong Stoner instability of the nonmagnetic phase that is numerically similar to that of nonmagnetic Fe.

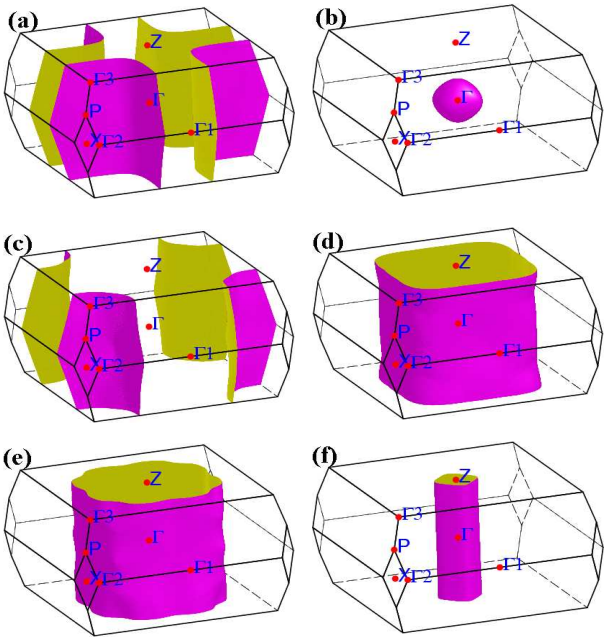

FIG. 6: (Color online) LDA FM Fermi surfaces, for M= 1.95 μ_B. Surfaces (a) and (b) are from the majority states, surfaces (c)-(f) from the minority bands. While (a) and (c) contain holes, the others enclose electrons. Each surface has mainly (a) $d_{x^2-y^2}$ (0.5 holes), (b) $d_{3z^2-r^2}$ (0.01 electrons), (c) d_{xz} (0.2 holes), (d) d_{xy} (0.4 electrons), (e) d_{yz} (0.4 electrons), and (f) $d_{x^2-y^2}$ (0.02 electrons) characters. The number in parentheses says carrier number containing each Fermi surface per Co.

C. Fermiology

The LDA FM Fermi surfaces (FS) pictured in Fig. 6 consist of two sheets from the majority states and four minority sheets, with very simple geometry and strong two-dimensionality. Except for one sheet that has an ellipsoidal shape (majority $d_{3z^2-r^2}$ character), the FSs have the shape of rectangular cylinders with rounded corners. The X-centered sheets

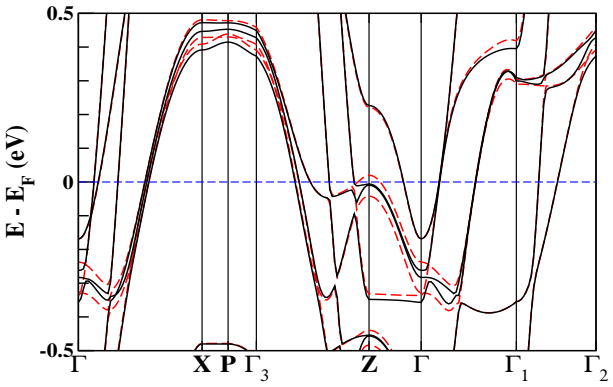

FIG. 7: (Color online) LDA FM band structures from spin-orbit coupling calculation with the quantization axis along ⟨100⟩ (solid) and ⟨001⟩ (dashed) directions. Note the ⟨001⟩ direction is the easy axis. The dashed horizontal line denotes the Fermi energy.

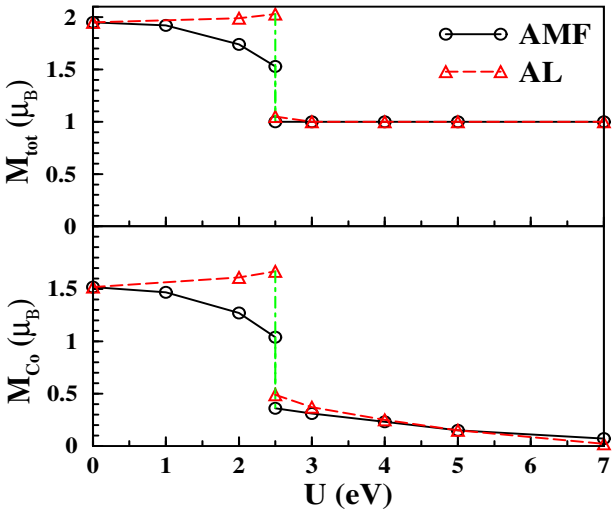

FIG. 8: (Color online) Effect of the on-site Coulomb repulsion U on total and Co local magnetic moments in both LDA+U schemes. At U_c=2.5 eV, a metal to half metal transition occurs. The first-order transition is obtained nearly at the same U in the both schemes. (In fact, the transition occurs a little higher U_c in FLL, but the difference is only less than a few tenth eV.)

contain holes, whereas the Γ-centered surfaces contain electrons. The FS arising from majority $d_{x^2-y^2}$ (Fig. 6(a)) has a clear nesting feature, as does the minority hole sheet in Fig. 6(d). The spanning vectors may lead to spin-density-wave or/and charge-density-wave instabilities. Intra-surface scattering may also show some nesting features. For the most part Fermi velocities v_F are in the range of a few 10^7 cm/sec as usual in a metal, but order of magnitude lower velocities occur along the Γ_3 to Z line at E_F.

D. Magnetocrystalline anisotropy

We included spin-orbit coupling by using the fully relativistic FPLO method[31] to allow us to study the strong magnetic anisotropy reported[14] by Matsuno *et al.* The total energies along ⟨100⟩ and ⟨001⟩ directions were calculated to determine the magnetocrystalline anisotropy energy (MAE). The energy difference $E_{\langle 100\rangle} - E_{\langle 001\rangle}$=0.57 meV/Co is consistent with experimentally observed ⟨001⟩ easy c-axis. The relativistic calculations give an orbital magnetic moment of 0.08 μ_B for Co, and negligible values for oxygen ions. The spin and orbital magnetic moments depend on the spin direction, differing by about 5%.

The experimental MAE can be estimated from field dependent magnetization along the two directions.[14] The data show half-saturation at 7 T along the ⟨100⟩ direction. Considering the saturated magnetization to be M_s=1.8 μ_B/Co, the MAE from $M_s \cdot B$ is 1.5 meV/Co, a value three times larger than our calculated result. Such underestimation in LDA is common for Co compounds. The reason is still unsettled, but candidate explanations are the poor treatment of orbital polarization[37] or for Hubbard-like correlation[38] in the standard LDA.

Rotating the spin direction induces a change of band structure, as shown Fig. 7. While the band structure for the moment along ⟨100⟩ direction is essentially that of LDA, there are additional splittings at several points for the moment oriented along the easy axis. The most visible splitting occurs in Co t_{2g} manifold, where the spin-orbit splitting spans E_F at the Z point. Applying SOC with spin directed along the easy axis, the bands split into primarily $d_{j=5/2,m_j=-3/2}$ character in the upper band, and $d_{j=3/2,m_j=1/2}$ in the lower band. The splittings are 60 meV and 90 meV at the Z and Γ point respectively.

IV. INCLUSION OF CORRELATION EFFECT

A. Metal to Half-metal Transition

Since the appropriate value of U in this and other cobaltate systems is unclear, we have studied the ground state as U is increased. The moment initially increases slightly in FLL, while it decreases slowly to 1.5 μ_B at U=2.5 eV in AMF, as shown in Fig. 8. From their separate states just below and at the critical value U_c=2.5 eV, beyond this critical value the

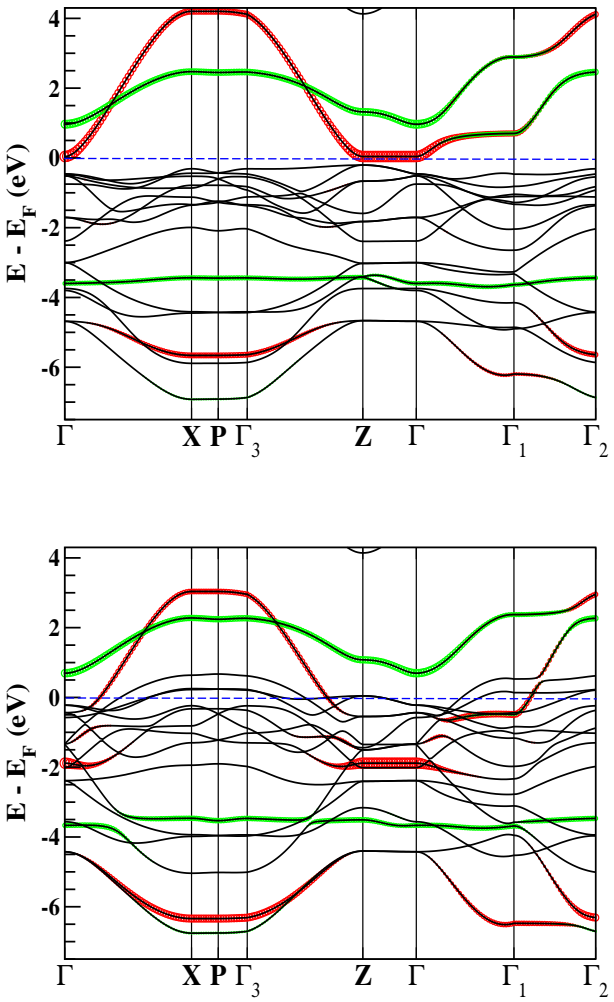

FIG. 9: (Color online) LDA+U FM majority (upper) and minority (lower) band structures at U_c=2.5 eV in the half metallic state with M=1 μ_B. The majority state shows a gap of 0.25 eV. The thickened (and colored) lines emphasize Co $d_{3z^2-r^2}$ (green or light) and $d_{x^2-y^2}$ (red or black) characters. The dashed horizontal line denotes the Fermi energy.

moment drops sharply to 1 μ_B in both schemes, and then both schemes produce very similar results in the entire region above U_c. Note particularly that this transition starts from distinct states, but occurs at the same value U_c to the same final state. Both high-moment and low-moment states can be stabilized in the calculations at U_c. Unlike studies in the Na_xCoO_2 system, no discernible hysteretic region could be found at this first-order transition. This magnetic collapse accompanies a metal to half metal transition, presumably because there is a particular stability of this half metallic (HM) FM state since both LDA+U schemes transition to it. The HM state, with a magnetic moment 1 μ_B, has been

TABLE II: Co 3d orbital occupancy in half metallic state, having M=1 μ_B, at U=2.5 eV. Compared with LDA result shown in Table I, there are two remarkable changes in the e_g state; nearly vanishing contribution of $d_{3z^2-r^2}$ and negative contribution of $d_{x^2-y^2}$ (for details, see text). It seems to be close to LS state, but the $d_{x^2-y^2}$ minority has considerable occupancy due to strong hybridization (itinerary) which makes impossible to be called strictly as LS state. The total occupation is 6.79.

	t_{2g}			e_g	
	E_g		B_{2g}	A_g	B_{1g}
	xz	yz	xy	$3z^2-r^2$	x^2-y^2
majority	1.00	1.00	1.01	0.35	0.25
minority	0.81	0.81	0.44	0.44	0.68
difference	0.19	0.19	0.57	-0.09	-0.43

observed also by Wang *et al.* As U increases, the Co local magnetic moment decreases to vanishingly small value by U ∼6-7 eV. The state remains a HM FM, the moment has been pushed onto the PO ions. Since the moment on Co has vanished, it is not surprising that the two LDA+U schemes give the same result.

The microscopic mechanism behind the magnetic collapse induced by the on-site Coulomb repulsion U can be unraveled from a study of the charge decompositions in Tables I and II, and comparison of band structures. We can compare and contrast the two viewpoints. First we point out that, while the Mullikan charges given in these tables are somewhat basis set dependent so their specific magnitude should not be given undue significance, differences – whether between orbitals or between spin-projections – are more physical. Then, while these orbital occupations provide one characterization, we have also provided in Figs. 2 and 9 by the fatbands technique, the bands that one identifies with $d_{x^2-y^2}$ and d_{3z^2-1} character. Using both viewpoints provides a more robust interpretation of behavior than either separately.

From the tables one can determine that increasing U does not change the total 3d occupation, but introduces rearrangements in the 3d charge and moment. From the bands, the main difference (between FM LDA and HM FM LDA+U) is that the dispersive majority $d_{x^2-y^2}$ band has become fully *un*occupied, leaving the small gap that results in half metallicity. Returning to the charges and moments, what stands out is that the moment on the $d_{x^2-y^2}$ orbital has flipped, from +0.35μ_B to -0.43μ_B. The d_{3z^2-1} moment has undergone a smaller change in the same manner: 0.20μ_B to -0.09μ_B. Thus the net

moment on the Co ion, which is $\sim 0.5\mu_B$, is the result of $\sim +1\mu_B$ in the t_{2g} orbitals (primarily d_{xy}) and $\sim -0.5\mu_B$ in the e_g orbitals. This type of cancellation, in more striking form, has been seen previously in LDA+U results for $LaNiO_2$,[40] which has an unusually *low* formal oxidation state for a nickelate.

B. Fixed Spin Moment Calculation at U_c

The results of the previous section show that two magnetic states coexist at U_c in LDA+U, whether one uses the AMF or FLL functional. Such a coexistence has been already observed in LDA+U calculations for the sodium cobaltates, where the change at U_c corresponds to a charge disproportionation transition.[39] Here the change is simply in the state of the (single) Co ion; there is no experimental indication of disproportionation here. Here we analyze the FSM results at U_c for LDA, AMF, and FLL.

The energy versus total magnetic moment behavior, displayed in Fig. 5, shows very interesting differences as well as similarities. Perhaps most interesting is that positions of local minima occur at (or near) integer values M=0, 1, and 2 (in units of μ_B), as if there might be underlying states with $S_z = 0$, $\frac{1}{2}$, or 1 pervading the behavior. The results of previous sections however established that there is strong $d-p$ hybridization which renders integral moments no more favored than other values. The LDA curve shows simple behavior: a Stoner instability at M=0 and a single minimum near (but not precisely at) M=2. The LDA+U results show more interesting variation.

For both AMF and FLL the paramagnetic state is metastable, with energy rising up to a moment $M \approx 0.5$, and then decreasing very similarly to the minimum at M=1. Beyond that point, AMF levels off to a broad flat region M=1.3–1.8 beyond which it increases with M. FLL however switches over to a separate phase, with its minimum at M=2. The E(M) curve for FLL seems to consist of two separate parabolas (different phases) with minima very near M=1 and M=2. The M=1 result is integral because a half metallic phase is encountered (see Fig. 9) and not due to an $S = 1/2$ configuration of the Co ion. Both majority $d_{x^2-y^2}$ and $d_{3z^2-r^2}$ become completely unoccupied, leaving a small gap to the t_{2g} bands.

We must point out that for both AMF and FLL schemes, the minimum at M=0 μ_B does not correspond to a nonmagnetic state. There is a moment on Co with magnitude 0.14 μ_B that is canceled by magnetization on the PO ion. The driving force for favoring this low, canceling moment phase over a nonmagnetic state is not clear. Possibly an antiferromagnetic result, requiring a doubled unit cell, would be a lower energy M=0 solution.

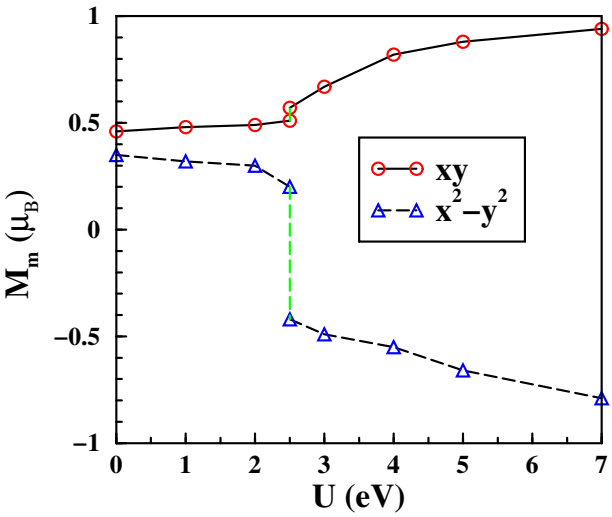

FIG. 10: (Color online) Effect of strength of U on the orbital-projected Co magnetic moment M_m, defined by difference between majority and minority occupancies, of Co $d_{x^2-y^2}$ and d_{xy} states in AMF scheme. (Results for the FLL scheme are similar.) In the large U limit an on-site "singlet" type cancellation of moments occurs in this $m = \pm 2$ channel (see Fig. 8 and text).

C. Strong Interaction Regime

In Sr_2CoO_4 correlation effects should not be very strong it seems, since LDA already gives a FM state that seems consistent with one of the experimental reports. However, in a strong correlated regime, but not beyond realistic range of U, there is another interesting feature. Figure 10 shows the U-dependent orbital-projected local magnetic moment M_m, defined by the difference between majority and minority occupancies, of Co $d_{x^2-y^2}$ and d_{xy} states. Upon increasing U, the d_{xy} minority state loses electrons, while the $d_{x^2-y^2}$ minority state gains electrons. Beyond $U = U_c = 2.5$ eV, d_{xy} and $d_{x^2-y^2}$ have large positive and negative local magnetic moments respectively, leading to an on-site "singlet" type cancellation within this $|m| = 2$ channel. This type of cancellation, but within the e_g manifold, has been seen already in our previous results for $LaNiO_2$.[40] In contrast with $LaNiO_2$, which shows the cancellation in the total magnetic moment and $Ni^{1+} \rightarrow Ni^{2+}$ conversion, the moment of the system remains unchanged because of large magnetic moments on planar oxygen ions.

V. SUMMARY

Synthesis of the high formal oxidation state compound Sr_2CoO_4, bulk materials by high-pressure high-temperature techniques and films by pulsed laser deposition (PLD), have led to a high Curie temperature metallic ferromagnet that introduces new transition metal oxide physics and may be useful in spin electronics devices. We have provided an in-depth study of the electronic and magnetic structure of this compound, looking specifically into the combined effects of correlation on the $3d$ orbitals and strong hybridization with O $2p$ states.

Within LDA Sr_2CoO_4 is metallic with a ferromagnetic moment near $2\mu_B$, close to the saturation magnetization reported for the PLD films. Application of the two commonly used LDA+U functionals reveals several surprises. As U is increased from zero, the two functionals produce changes in the moment of opposite sign up to the critical value U_c=2.5 eV. Beyond half metallic ferromagnetic phase with moment $1\mu_B$. Within this phase, increasing the value of U has the effect of pushing the moment completely off the Co and onto the planar O ions by $U \sim$ 6-7 eV, while the total moment remains fixed at $1\mu_B$.

With U fixed at U_c=2.5 eV, fixed spin moment calculations were carried out for both LDA+U functionals, and compared with the corresponding LDA result. Both LDA+U schemes behaved similarly out to a minimum at $1\mu_B$ (the half metallic state). Beyond this the two functionals departed in their behavior, with the FLL scheme jumping to a new state with minimum very near $2\mu_B$, not half metallic and much the same as the LDA minimum ($1.95\mu_B$). In the stronger-interacting regime $U \geq 3$ eV (which may not be appropriate for Sr_2CoO_4), the correlation described by the LDA+U approach leads to oppositely directed moments on the $d_{x^2-y^2}$ and d_{xy} orbitals, reflecting the strong difference in hybridization of these two orbitals.

VI. ACKNOWLEDGMENTS

We acknowledge illuminating conversations with M. Richter for magnetic anisotropy energy and K. Koepernik for technical assistance. This work was supported by DOE grant DE-FG03-01ER45876 and DOE's Computational Materials Science Network. W.E.P. acknowledges the stimulating influence of DOE's Stockpile Stewardship Academic Alliance Program.

[1] K. Takada, H. Sakurai, E. Takayama-Muromachi, F. Izumi, R. A. Dilanian, and T. Sasaki, Nature **422**, 53 (2003).
[2] M. L. Foo, Y. Wang, S. Watauchi, H. W. Zandbergen, T. He, R. J. Cava, and N. P. Ong, Phys. Rev. Lett. **92**, 247001 (2004).
[3] G. C. Amatucci, J. M. Tarascon, and L. C. Klein, J. Electrochem. Soc. **143**, 1114 (1996); J. M. Tarascon, G. Vaughan, Y. Chabre, L. Seguin, M. Anne, P. Strobel, and G. Amatucci, J. Solid State Chem. **147**, 410 (1999).
[4] A. Van der Ven, M. K. Aydinol, G. Ceder, G. Kresse, and J. Hafner, Phys. Rev. B **58**, 2975 (1998).
[5] T. Matsurra, J. Tabuchi, J. Mizusaki, S. Yamauchi, and K. Fueki, J. Phys. Chem. Solids **49**, 1403 (1988).
[6] Y. Furukawa, S. Wada, and Y. Yamada, J. Phys. Soc. Jpn. **62**, 1127 (1993).
[7] Y. Moritomo, K. Higashi, K. Matsuda, and A. Nakamura, Phys. Rev. B **55**, 14725(R) (1997).
[8] J. Wang, W. Zhang, and D. Y. Xing, Phys. Rev. B **62**, 14140 (2000).
[9] M. Sanchez-Andujar, B. Rivas-Murias, D. Rinaldi, R. Caciuffo, J. Mira, R. Rivas, and M. A. Senaris-Rodriguez, J. Magn. Magn. Mat. **272-276**, 855 (2004).
[10] G. Demazeau, P. Courbin, G. L. Flem, M. Pouchard, P. Hagenmuller, J. L. Soubeyroux, I. G. Main, and G. A. Robins, Nouv. J. Chim. **3**, 171 (1979).
[11] Y.Y. Liu, X.M. Chen, and X.Q. Liu, Solid State Commun. **136**, 576 (2005).
[12] C. N. R. Rao, P. Ganguly, K. K. Singh, and R. A. Mohan Ram, J. Solid State Chem. **72**, 14 (1988).
[13] K. Yamada, M. Matsuda, Y. Endoh, B. Keimer, R. J. Birgeneau, S. Onodera, J. Mizusaki, T. Matsuura, and G. Shirane, Phys. Rev. B **39**, 2336 (1989).
[14] J. Matsuno, Y. Okimoto, Z. Fang, X. Z. Yu, Y. Matsui, N. Nagaosa, M. Kawasaki, and Y. Tokura, Phys. Rev. Lett. **93**, 167202 (2004).
[15] J. Matsuno, Y. Okimoto, Z. Fang, X. Z. Yu, Y. Matsui, N. Nagaosa, H. Kumigashira, M. Oshina, M. Kawasaki, and Y. Tokura, Thin Solid Films **486**, 113 (2005).
[16] X. L. Wang and E. Takayama-Muromachi, Phys. Rev. B **72**, 064401 (2005).
[17] X. L. Wang, H. Sakurai, and E. Takayama-Muromachi, J. Appl. Phys. **97**, 10M519 (2005).
[18] T. Tekeda, T. Watanabe, S. Komura, and H. Fujii, J. Phys. Soc. Jpn. **56**, 731 (1987).
[19] S. Mathi Jaya, R. Jagadish, R. S. Rao, and R. Asokamani, Phys. Rev. B **43**, 13274 (1991).
[20] R. H. Potze, G. A. Sawatzky, and M. Abbate, Phys. Rev. B **51**, 11501 (1995).
[21] M. A. Korotin, S. Yu. Ezhov, I. V. Solovyev, V. I. Anisimov, D. I. Khomskii, and G. A. Sawatzky, Phys. Rev. B **54**, 5309 (1996).
[22] H. Takahashi, F. Munakata, and M. Yamanaka,

Phys. Rev. B **57**, 15211 (1998).
[23] I. A. Nekrasov, S. V. Streltsov, M. A. Korotin, and V. I. Anisimov, Phys. Rev. B **68**, 235113 (2003).
[24] G. Maris, Y. Ren, V. Volotchaev, C. Zobel, T. Lorenz, and T. T. M. Palstra, Phys. Rev. B **67**, 224423 (2003).
[25] D. Phelan, Despina Louca, S. Rosenkranz, S.-H. Lee, Y. Qiu, P. J. Chupas, R. Osborn, H. Zheng, J. F. Mitchell, J. R. D. Copley, J. L. Sarrao, and Y. Moritomo, Phys. Rev. Lett. 96, 027201 (2006).
[26] For a review, see V. I. Anisimov, F. Aryasetiawan, and A. I. Lichtenstein, J. Phys.: Condens. Matter **9**, 767 (1997).
[27] K. Koepernik and H. Eschrig, Phys. Rev. B **59**, 1743 (1999).
[28] V. I. Anisimov, I. V. Solovyev, M. A. Korotin, M. T. Czyzyk, and G. A. Sawatzky, Phys. Rev. B **48**, 16929 (1993).
[29] M. T. Czyzyk and G. A. Sawatzky, Phys. Rev. B **49**, 14211 (1994).
[30] S. L. Dudarev, G. A. Botton, S. Y. Savrasov, C. J. Humphreys, and A. P. Sutton, Phys. Rev. B **57**, 1505 (1998).
[31] H. Eschrig, M. Richter, and I. Opahle, in *Relativistic Electronic Structure Theory - Part II: Applications*, edited by P. Schwerdtfeger (Elsevier, Amsterdam, 2004), pp. 723-776.
[32] K. Schwarz and P. Mohn, J. Phys. F: Met. Phys. **49**, L129 (1984).
[33] L. F. Mattheiss, Phys. Rev. Lett. **58**, 1028 (1987).
[34] For review, see W. E. Pickett, Rev. Mod. Phys. **61**, 433 (1989).
[35] K.-W. Lee and W. E. Pickett, J. Appl. Phys. (to be published); cond-mat/0508649.
[36] R. Weht and W. E. Pickett, Phys. Rev. Lett. **81**, 2502 (1998).
[37] H. Eschrig, M. Sargolzaei, K. Koepernik, and M. Richter, Europhys. Lett. **72**, 611 (2005).
[38] D. Mertz, R. Hayn, I. Opahle, and H. Rosner, Phys. Rev. B **72**, 085133 (2005).
[39] K.-W. Lee, J. Kuneš, P. Novak, and W. E. Pickett, Phys. Rev. Lett. 94, 026403 (2005).
[40] K.-W. Lee and W. E. Pickett, Phys. Rev. B **70**, 165109 (2004).